Journal of Sol-Gel Science and Technology (2021) 97:245–258
https://doi.org/10.1007/s10971-020-05442-5

ORIGINAL PAPER: CHARACTERIZATION METHODS OF SOL-GEL AND HYBRID MATERIALS

Synthesis and characterization of nanoparticulate niobium- and zinc-doped bioglass-ceramic/chitosan hybrids for dental applications

Vuk Uskoković[1] · Gabriel Abuna[2] · Paulo Ferreira[3] · Victoria M. Wu[4] · Laurie Gower[5] · Fernanda Carvalho Panzeri Pires-de-Souza[6] · Ramiro Mendonca Murata[2] · Mario Alexandre Coelho Sinhoreti[3] · Saulo Geraldeli[2]

Received: 19 June 2020 / Accepted: 4 November 2020 / Published online: 7 January 2021

Abstract

Dental caries and periodontal disease are responsible for the most frequent set of chronic diseases in humans, for which no perfectly regenerative solutions are available yet. As a result, materials combining an intrinsic antibacterial activity with tissue regeneration properties for minimally invasive dental therapies are in high demand. Here we report on the fabrication and characterization of a novel nanocomposite material for such dental applications. The material is composed of narrowly disperse Na_2O–CaO–P_2O_5–SiO_2 bioglass-ceramic nanoparticles, 30–70 nm in diameter, doped with antibacterial and osteogenic zinc and niobium ions, and hybridized with chitosan. These systems were characterized for their particle size, morphology, atomic and phase composition, and glass-ceramic/polymer interface with the use of transmission electron microscopy, energy-dispersive X-ray analysis, X-ray diffraction and Fourier transform infrared spectroscopy. After annealing at 680 °C, amorphous silica in the bioglass-ceramic coexisted with silicalite-1 and combeite, the average crystallite size of which was 20–40 nm. In spite of the significantly better incorporation of zinc than of niobium inside the glass-ceramic network, zinc did not affect the particle size and shape distribution, while niobium lowered the average particle size. Chitosan increased the hydration capacity of the bioglass-ceramic and it formed a continuous interface around the bioglass-ceramic nanoparticles, devoid of micropores. This intimacy of the interface was confirmed by the downshift of the critical Si–O(–Si) vibration modes in the bioglass-ceramic upon hybridization with chitosan. The addition of zinc ions hampered the partial recrystallization during annealing by interfering with the Si–O network restructuring, in direct proportion with its concentration. Niobium ions produced a similar structure-breaking effect, which was evidenced, as in the case of zinc, by upshifting the antisymmetric Si–O–Si stretch of the bridging oxygen and increasing the full-width at half maxima for all the major Si–O(–Si) vibration modes. The effective electrostatic attraction between the aminated hydrocarbon chains of chitosan and the negatively charged silanol groups of silica may extend to the interaction with dentin collagen fibrils decalcified due to caries, making the material of potential interest for adhesive fillers of cariogenic lesions in teeth. Both the undoped and the doped bioactive glass-ceramics interacted favorably with odontoblast-like cells, accentuating their potential for further research for applications in minimally invasive reparative dentistry.

✉ Vuk Uskoković
vuk21@yahoo.com

[1] TardigradeNano, Irvine, CA 92604, USA

[2] School of Dental Medicine, East Carolina University, Greenville, NC 27834, USA

[3] Department of Restorative Dentistry, Piracicaba Dental School, Campinas State University, Piracicaba, SP 13414-903, Brazil

[4] MP Biomedicals, Irvine, CA 92618, USA

[5] Department of Materials Science & Engineering, University of Florida, Gainesville, FL 32611, USA

[6] Department of Dental Materials and Prosthodontics, Ribeirao Preto School of Dentistry, University of Sao Paulo, Ribeirão Preto, SP 14040-904, Brazil

Graphical Abstract

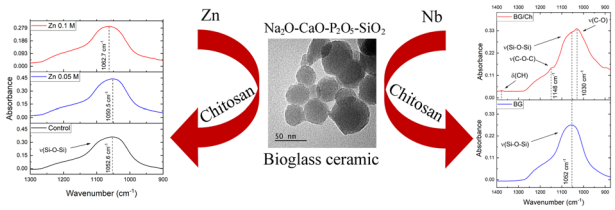

Keywords Bioglass · Dentistry · Doping · FTIR · Odontoblasts · XRD

Highlights

- Chitosan-coated Zn- or Nb-doped Na_2O–CaO–P_2O_5–SiO_2 bioglass ceramic was synthesized and characterized.
- Chitosan increased the hydration capacity and formed a continuous interface around the nanoparticles.
- Zn hampered the recovery during annealing and Nb promoted it.
- Both Zn and Nb exhibited structure-breaking effects on the Si–O–Si glassy network.
- Zn-doped material was less viable to odontoblasts than the control and the Nb-doped one at low dosages.

1 Introduction

The rapid evolution of resistance of pathogenic microorganisms to the current generation of small-molecule antibiotics has elicited the search for alternative therapies to suppress infectious diseases and prevent potentially devastating pandemics [1]. One of the most prospective alternatives to small-molecule antibiotics are antibacterial inorganics [2], including materials doped with ions with pronounced antibacterial activities [3]. Albeit less bactericidal and targeted in terms of the mechanism of action, such ions are less prone to induce the resistance in pathogenic bacterial species than their molecular analogs [4].

In restorative dentistry, secondary caries is one of the main causes for failure of resin-based composite restoration. One of the fundamental reasons for this lies in the lack of any intrinsic antimicrobial capacity of their ingredients, which severely affects the long-term intraoral service performance of the material [5]. Another reason is that no restorative formulations are composed of nanoparticles small enough to penetrate dentinal tubules and peritubular dentin degraded by the cariogenic bacteria. As a result, nanoscale materials combining an intrinsic antibacterial activity with tissue regeneration properties are in constant demand. All mineralized dental tissues are composite in nature, combining a soft, protein-based matrix with a hard, apatite component [6]. While enamel contains only trace amounts of the organics, dentin and cementum resemble bone in their more balanced weight ratio between the soft and the hard components. Therefore, it is conceivable that a restorative material designed to treat disease-affected dental tissues should, at least in principle, imitate the composition of such organic/ceramic hybrids [7].

Bioglass has the well-known ability to stimulate the regeneration of hard tissues [8], including the remineralization of teeth [9]. As per the Kokubo bioactivity study assay [10], bioglass can precipitate apatite on its surface when immersed in biological fluids, which is one of the factors favoring hard tissue regeneration [11]. Different formulations of bioglass and bioglass-ceramics have been used for half a century now to repair bone and dental defects, while more recent research has expanded bioglass to new domains, such as soft tissue repair and drug delivery [12].

Unlike bioglass and bioglass-ceramics, which are synthetic products, chitosan is a derivative of chitin, a naturally occurring biopolymer and the second most abundant polysaccharide after cellulose. It is the polymer-matrix frequently used for scaffolds or drug delivery carriers because it is biocompatible and enzymatically degradable. In comparison with polyesters, its high density of constitutive amine groups endows chitosan with a cationic nature and thus with the capacity to display excellent muco-adhesion, in situ gelation, antimicrobial properties, the ability to permeate the intestinal epithelium and other biological barriers, as well as the ability to display smart, pH-controlled dissolution and drug release properties [13]. Chitosan can also be processed in various forms, including nanoparticles, microspheres, thin films, hydrogels, nanofibers, nanocomposites, and so on [14]. Its antibacterial effect against cariogenic *S. mutans* and the ability to resist biofilm formation are also notable [15–17], which has put it on the list of useful polymers for dental applications.

Zn is an essential microelement in the human body, where it is involved in several protein, carbohydrate, lipid and bone metabolic processes. It acts as a cofactor in

enzymatic reactions and is the integral constituent of zinc-finger protein domains. Its importance for cell growth and differentiation, in fact, have made it the most intensely studied microelement in newborn nutrition [18]. Its physiological concentrations are tightly regulated and deficiencies in puerility can lead to symptoms such as stomatitis, glossitis, alopecia, growth retardation, dwarfism, immunosuppression, and depression [19]. In addition to this, Zn ions are noted for their antibacterial properties, which they exhibit against a broad spectrum of bacterial species [20]. Zn can also replace calcium ions in the hydroxyapatite lattice and has been shown to reduce the dissolution rate of enamel upon its accommodation in it [21]. Zinc is naturally present in saliva and is also added to toothpastes and mouthwashes to reduce calculus formation and prevent caries by mechanisms that include increased acid attack resistance of the apatite lattice [22, 23], hopeite formation [24] and adsorption on crystal surface kinks [25] to block the dissolution and promote remineralization. Interestingly, while fluoride is more effective in preventing the demineralization of sound enamel, zinc appears to be more effective in preventing the demineralization of preformed lesions in enamel [26]. These findings imply that while F may still be a good choice to halt the formation of cariogenic lesions in enamel, Zn may be a more effective ion to use to prevent the progression of preexistent cariogenic lesions [27]. Concordantly, we hypothesize that Zn is a good choice for use in the design and development of new materials for the minimally invasive repair of demineralized dental tissues. This hypothesis is strengthened by the known angiogenic and osteogenic potential of Zn ions [28, 29] as well as by their integration to hard tissues deposited by odontoblasts [30] and pulpal cells [31].

Unlike the endogenous Zn, Nb is a chemical element completely foreign to the human body, having no known functions in it. It is also a markedly less explored element for antibacterial and other biological applications. Still, limited prior studies did show that potassium sodium niobate ($K_{0.5}Na_{0.5}NbO_3$) piezoceramics can decrease the growth of Gram-positive *S. aureus* colonies and increase the mesenchymal stem cell proliferation [32], even though potassium hexaniobate ($K_4Nb_6O_{17}$) did not show any activity against Gram-negative *E. coli* [33]. The addition of niobium pentoxide (Nb_2O_5) also increased the bioactivity of gelatin/alginate membranes [34]. Still, more studies are needed to confirm the biocompatibility and the antibacterial capacity of Nb-containing biomaterials.

In this study we report on the synthesis of novel ion-doped bioglass-ceramic/chitosan nanoparticles as potential ingredients of dental biomaterials and other medical devices designed to simultaneously halt the bacterial growth and remineralize the demineralized tissue. We foresee that the intrinsic antibacterial properties of one such novel nanocomposite would be owed to the combination of chitosan and doping with antimicrobial ions, thereby overcoming the need for the use of small-molecule inhibitors of bacterial growth. Specifically, here we use two ionic dopants, niobium (Nb) and zinc (Zn), accommodated inside the amorphous phase and the crystalline lattice of bioglass-ceramic nanoparticles distributed within the polymeric matrix composed of chitosan. In addition to the utilization of potentially antimicrobial and osteogenic Nb and Zn ions, the core bioglass-ceramic nanoparticles were designed to contain both calcium and phosphate ions, with the idea that these constitutive ions would present the growth units for the crystallization of hydroxyapatite, thereby enabling remineralization of any remnant demineralized regions of the tooth. The material is synthesized in a multistep process using wet chemistry and characterized for its phase composition, particle size, morphology and interaction between its two components, namely bioglass-ceramic and chitosan.

2 Materials & methods

2.1 Bioglass-ceramic nanoparticle synthesis

The synthesis of a four-component Na_2O–CaO–P_2O_5–SiO_2 bioglass powder was achieved with a modified Stöber process using calcium nitrate ($Ca(NO_3)_2{\cdot}4H_2O$), sodium nitrate ($NaNO_3$), triethyl phosphate ($(C_2H_5)_3PO_4$) and tetraethyl orthosilicate ($Si(OC_2H_5)_4$, reagent grade, 98 %, TEOS) as the reagents and ammonium hydroxide (ACS reagent, 28.0–30.0% NH_3 basis) as the catalyst. In a round-bottom vessel as the reaction beaker, TEOS was added to the solution containing 200 ml of deionized water and 1 M ammonium hydroxide. The addition of the reagents to the TEOS solution was in the following order: $(C_2H_5)_3PO_4$, $NaNO_3$ and $Ca(NO_3)_2\ 4H_2O$. The reaction mixture was kept under constant stirring with a magnetic bar for 3 h at 60 °C. The solution containing the bioglass precipitate was then centrifuged and washed with ethanol and distilled (DI) water 3 times at 3500 rpm for 2 min. The supernatant was removed, and the solid pellet dried in an oven at 60 °C for 24 h under vacuum. To obtained the bioglass-ceramic, the samples were annealed at 680 °C for 3 h. These thermal treatment parameters were selected to optimally remove nitrates and incorporate calcium ions into the silica glassy network without full crystallization. Synthesis of Zn- and Nb-modified bioglass-ceramic by means of partial calcium replacement was done by adding zinc sulfate ($ZnSO_4$) and niobium oxalate ($C_2H_2NbO_4$) in the 2.5 mol.% concentration range to the TEOS solution.

2.2 Bioglass-ceramic/chitosan nanoparticle synthesis

To hybridize the as-synthesized bioglass-ceramic particles with chitosan, 10 mg of the bioglass-ceramic powder was

suspended in 40 ml water adjusted to pH 10 with the dropwise addition of nM concentration NaOH, and 2 ml of a 1 mg/ml aqueous solution of chitosan (poly(D-glucosamine) deacetylated chitin, $M_w = 190–310$ kDa; Sigma) containing 30 mM HCl was added dropwise to the magnetically stirred sol. The precipitate alongside its parent solution was left to age under atmospheric conditions for 1 h. After the given time, the precipitate was washed with DI water, centrifuged for 5 min at 3500 rpm, and dried in a vacuum oven (Isotemp 280 A; $p = -20$ mmHg) at 60 °C.

2.3 Physicochemical characterization

Transmission electron microscopy (TEM) analysis was carried out to examine the morphology of the bioglass-ceramic particles incorporating different ionic additives (Nb and Zn) and hybridized with chitosan. The bioglass-ceramic powders were suspended in water, then picked up on Cu grids under the microscope and imaged on a transmission electron microscope (Tecnai BioTWIN, FEI, Hillsboro, OR) at an accelerating voltage of 80 kV [35].

X-Ray diffraction (XRD) studies were carried out on a Bruker D2 Phaser diffractometer using polychromatic Cu as the irradiation source. K_β line was stripped off with an inbuilt filter, whereas $K_{\alpha 2}$ line was stripped off manually. Scanning conditions were the step size of 0.02° and 314 s of irradiation time ($\lambda = 1.5416$ A) per step. The average crystallite size, d, was estimated by applying the Debye–Scherrer equation on the half-width of the (002) diffraction peak of chitosan expressed in radians ($\beta_{1/2}$), using 1.5418 Å as the wavelength of $Cu_{K\alpha}$ as the radiation source (λ):

$$d = 0.94\lambda/\beta_{1/2}\cos\theta \quad (1)$$

Fourier transform infrared (FTIR) analysis was performed on a Bruker Alpha Platinum attenuated total reflection (ATR) spectrometer with a single-reflection diamond/WC composite ATR module. The full width at half maximum (FWHM) and the centers of the integrated major infrared bands were measured using an automated multiple peak-fitting Gaussian routine (*OriginPro 2018*). Bioglass-ceramic/chitosan samples prepared using different concentrations of dopant precursor solutions, including 0.1 M for Nb and 0.05 and 0.1 M for Zn, were subjected to the analysis.

2.4 Cell viability assay

The cell viability assays were performed on odontoblast-like MDPC-23 cells. MDPC-23 cells were cultured in a cell culture medium (Corning® DMEM [+] 4.5 g/L glucose, L-glutamine [−] sodium pyruvate) containing 8% of fetal bovine serum (GenClone™ FetalPURE™ 100% U.S. Origin Bovine Serum, Heat Inactivated) and 1% L-glutamine: penicillin:streptomycin solution at 37 °C in 5% CO_2. All experiments were performed with cells within 7th to 9th passages. For each experiment, the same passage of cells was used. A total of 1×10^5 of cells were seeded in each 96-well plate. Individual plates seeded with cells were then divided to the following experimental groups: (i) No material (Control); (ii) Material serially diluted to concentrations of 10000, 1000, 100, 10, 1 and 0.1 µg/mL of particles in DMEM; (iii) No cells and 10,000 µg/mL of the particles. All experiments were conducted in triplicates for each group/concentration.

The cell survival was assessed after 24 h of direct contact with the particles using CellTiter-Blue Cell Viability Assay (Promega). The reagent was added to each 96-well plate media for all the sample groups and incubated for 3 h at 37 °C and 5% CO_2. The fluorescence was measured at 570 nm using a spectrophotometric microplate reader (Molecular Devices). After viability was determinated in terms of percentages compared to the raw absorbance of control wells, the IC_{50} was obtained using GraphPad Prism 8.0 assessing the Log[Dose inhibitor] variable slope. The results were analyzed with a Normality test, after which a t-test among the groups and One-way ANOVA were used to statistically compare them. The test was performed using the significance level, α, of 0.05.

2.5 Antimicrobial activity assay

The zone of inhibition was determined by agar diffusion method using Trypsin Soy Agar (TSA). Isolated 24 h colonies of *Streptococcus mutans* (UA159) were suspended in sterile phosphate buffer solution. The suspension was adjusted spectrophotometrically to match the turbidity of a McFarland 0.5 scale. The inoculum (10^5 CFU/mL) procedures were appropriate to provide semiconfluent growth of the microorganism on TSA plates. Four sterilized glass cylinders with internal diameters of 5 mm and external diameters of 7 mm were placed on each inoculated agar plate. Ten milligrams of each nanoparticle powder were used to fill three cylinders, while the fourth cylinder was filled with a 10 µL solution of 0.12% chlorhexidine, which acted as a positive control. The plates were incubated at 37 °C in 5% CO_2 for 24 h. The zones of inhibition due to microbial growth around the cylinder containing the nanoparticles were measured and recorded after the incubation time was over. The inhibitory zone was considered as the shortest distance (mm) from the outside margin of the cylinder to the initial point of the microbial growth.

Minimal inhibitory concentration (MIC) and minimal bactericidal concentration (MBC) were determined by broth microdilution method [36]. Serially diluted treatments of the three nanoparticles were mixed with the TSB medium and added to wells of 96 well plates. The highest concentration

was 10,000 µg/mL, decreasing tenfold until 0.1 µg/mL, was used and added to a suspension of *S. mutans* containing 10^5 CFU/mL in each well ($n = 6$). Next, the plates were incubated at 37 °C and 5% CO_2 for 24 h to evaluate the MIC, which was defined as the lowest concentration of nanoparticles that had restricted growth to a level of $p \leq 0.05$ at 660 nm (no visible growth). To determine the MBC, an aliquot (50 µL) of all incubated tested groups was subcultured on TSA and incubated at 37 °C, 5% CO_2, for 48 h. The MBC was defined as the lowest concentration of nanoparticles that resulted in no bacterial growth on the agar (99.9% killed).

3 Results and discussion

Spherical and monodisperse particles present one of the most sought after types of particles for application as dental fillings and bone grafts in dental and orthopedic medicine [37, 38]. Namely, sphericity and monodispersity directly translate to the reproducibility of the treatment and ensure an even distribution of the effect of the nanoparticles on every region of the living tissue that comes into contact with them [39]. Bioglass-ceramic particles without any dopants were exactly such: round with a narrow size distribution (Fig. 1). Low-magnification TEM images show evidence of their disperse appearance on the formvar grid as irregularly shaped agglomerates (Fig. 1a), but at higher magnification, it is evident that that the degree of agglomeration is moderate, allowing the particles to preserve their individuality and characteristic spherical shapes (Fig. 1b, c). Despite the annealing at 680 °C, no sintering and coalescence of particles were observed. The particle size was in the 25–70 nm range (Fig. 1d), which is, theoretically, small enough to allow the particles to penetrate dentinal tubules and peritubular dentin, providing an easy access to the vicinity of collagen fibrils that become demineralized due to the acid attack by cariogenic bacteria. This theoretical ability is a fundamental prerequisite for an ideal, noninvasive and effective self-healing biomimetic remineralization strategy. Our current work stems from the effort to create and test one such healing capacity in a biomaterial for clinical dental applications.

Doping with Zn or Nb, interestingly, had a very different effect on the bioglass-ceramic particle size distribution. Specifically, as it can be seen from TEM images shown in Fig. 2, while the doping with Zn did not affect this size distribution, doping with Nb significantly lowered the average particle size in the regions where measurable concentration of Nb were detected. This was in spite of the 25 times higher concentration of Zn in the Zn-doped bioglass-ceramic than the concentration of Nb in the Nb-doped bioglass-ceramic (Table 1). The explanation to this effect could be sought in the possibility emerging from earlier studies [40] that Nb_2O_5 may be the first crystalline phase to form from the amorphous glass during annealing, preceding the crystallization of Si–, Na– or Ca–O networks. As a result, Nb_2O_5 may be expected to decrease the crystallization temperature of a ceramic glass in direct proportion with its content [41]. This early formation of Nb_2O_5 theoretically allows it to affect the nucleation and crystal growth of its complementary phases and thus the particle parameters such as size and morphology. The favorable formation of calcium niobate ($Ca_2Nb_2O_7$) as the secondary phase in the intergranular areas [42] is another effect that may have played a role in accelerating the crystallization and diminishing the average particle size. Other crystalline phases comprising Nb, e.g., $Na_4Nb_8P_4O_{32}$ or $NaNbO_3$, were also detected as the most stable crystalline pockets in Nb-containing glass-ceramics [43], implying their early, energetically favorable formation and a potential role as nucleation surfaces that alter the crystallization mechanism and/or rate. Another interesting effect observed from the EDX elemental analysis was the twice more abundant incorporation of calcium ions into the Zn-doped glass-ceramic than into its Nb-glass analog (Table 1).

After the hybridization with chitosan, the bioglass-ceramic nanoparticles became partially or completely encapsulated within the polymeric matrix (Figs 3 and 4). The great majority of the polymeric phase was detected

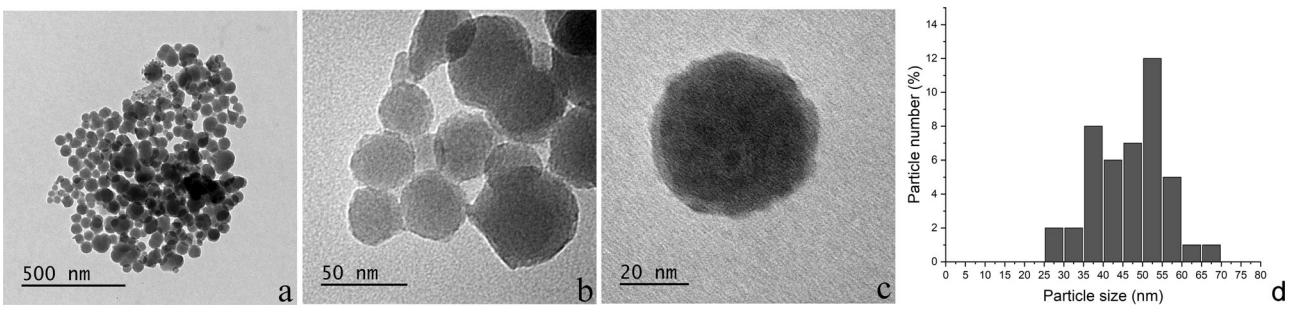

Fig. 1 TEM images of control, undoped bioglass-ceramic nanoparticles at different magnifications, ranging from the lowest (**a**) to the highest (**c**), depicting the nanoparticle agglomeration, morphology and size. The particle size distribution histogram is shown in **d**

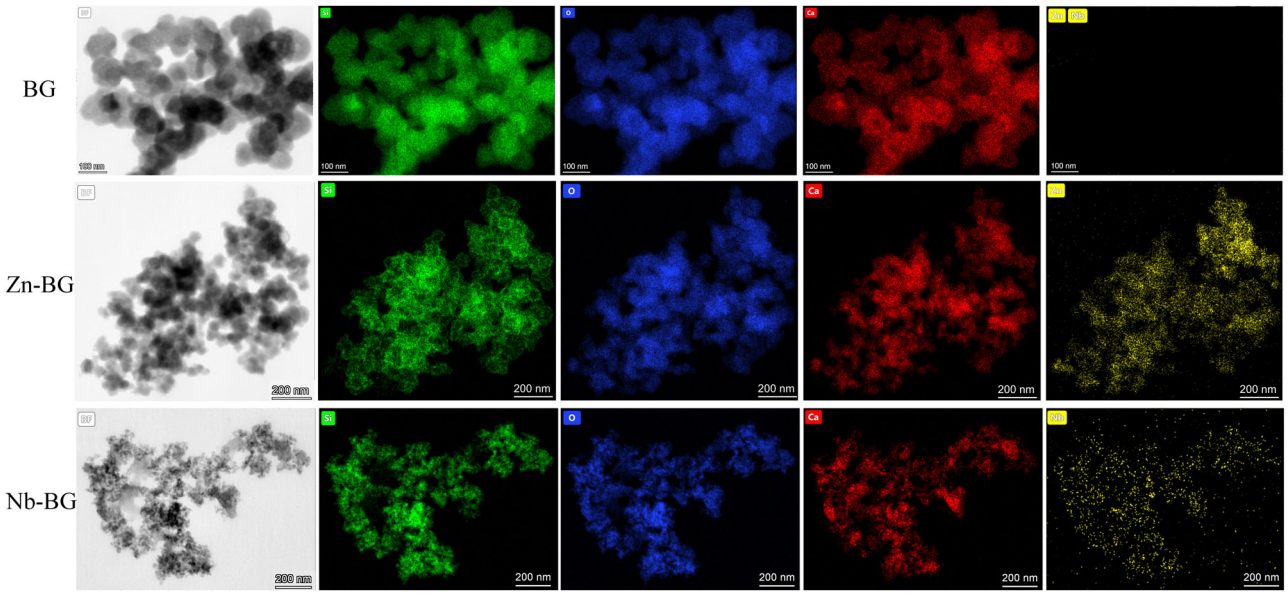

Fig. 2 TEM/EDX mapping analysis of control, undoped bioglass-ceramic nanoparticles (BG) and of bioglass-ceramic nanoparticles doped with Zn (Zn-BG) of Nb (Nb-BG) for different atomic elements, including Si, O, Ca, and Zn/Nb (left to right)

Table 1 Elemental analysis of control, undoped bioglass-ceramic nanoparticles (BG) and of bioglass-ceramic nanoparticles doped with Zn (Zn-BG) or Nb (Nb-BG) based on the intensity of K_α lines in the EDX analyses

Sample	Si (at.%)	O (at.%)	Ca (at.%)	Zn (at.%)	Nb (at.%)
BG	39.3	51.9	8.8	/	/
Zn-BG	23.9	58.4	12.4	5.3	/
Nb-BG	33.4	60.1	6.3	/	0.2

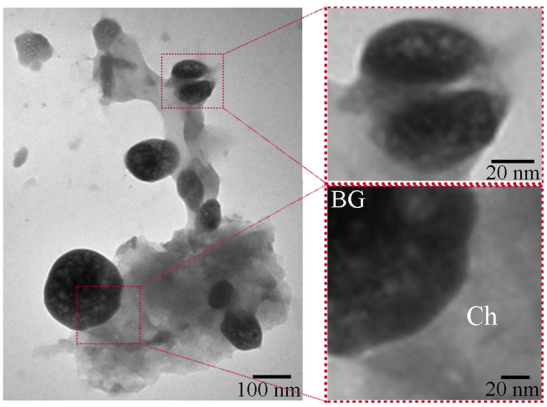

Fig. 3 TEM images of Zn-doped bioglass-ceramic nanoparticles coated with chitosan. Chitosan (Ch) and bioglass-ceramic (BG) are labeled in the bottom right image

adjacent to the surface of the bioglass-ceramic, indicating a favorable attraction between the two. In the regions of complete encapsulation of the bioglass-ceramic nanoparticles by the polymer, the interface between the phases

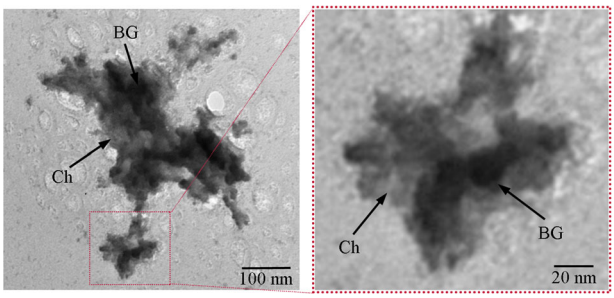

Fig. 4 TEM images of Nb-doped bioglass-ceramic nanoparticles coated with chitosan. Chitosan (Ch) matrix and bioglass-ceramic (BG) nanoparticles are marked with black arrows. The splotchy appearance of the background likely originates from beam damage and contraction of the chitosan matrix

was continuous, uninterrupted and devoid of micropores (Fig. 3). Occasionally, chitosan appeared to act as a bonding agent between pairs of adjacent bioglass-ceramic particles (Fig. 3). Earlier studies show analogous findings by demonstrating that chitosan could have useful properties as an adhesive, especially after appropriate chemical modifications that increase its hydrophobicity, such as hydrocaffeic acidification [44], alkylation [45] or catechol group addition [46]. With secondary caries being primarily caused by the degradation of the interface between the tooth and the adhesive joint and the formation of crevices that get colonized by cariogenic pathogens, an advantage of the soft chitosan matrix would come from its swelling into a hydrogel when placed in the physiologic fluid of the dentin cavity, creating a tight and conformal interface between the nanocomposite and the surrounding dental tissue [47].

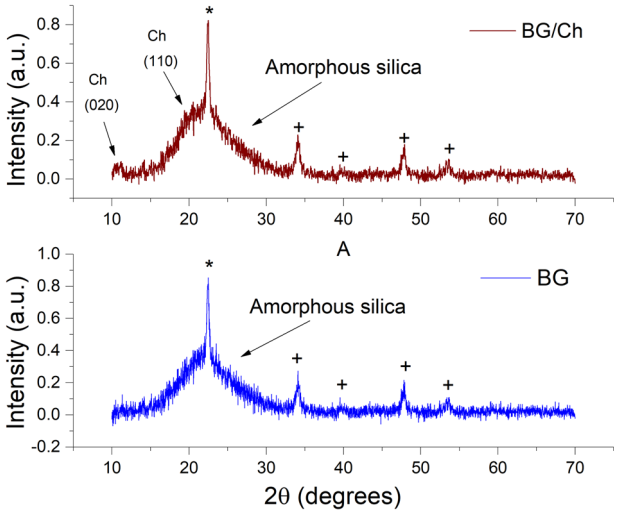

Fig. 5 XRD patterns of the control, undoped bioglass-ceramic (BG) and of its hybrid with chitosan (BG/Ch). The single silicalite-1 reflection is denoted with *, while combeite reflections are denoted with +. Chitosan reflections are denoted with Ch and with their corresponding Miller indices

The electrostatic attraction between the aminated hydrocarbon chains of chitosan on one side and the negatively charged silanol groups of silica and/or the collagenous network of dentin on the other is anticipated to strengthen this contact and allow it to be maintained during the stages of ionic release and bioactive remineralization.

XRD was used for the phase composition analysis of pure bioglass-ceramic and its hybrid with chitosan. Figure 5 shows the XRD patterns of both materials, while the results of the quantitative analysis of the bioglass-ceramic component are presented in Table 2. The most abundant phase, at 42.6 wt.%, is the silicalite-1 polymorph of silicon dioxide crystallizing in the orthorhombic structure and Pnma space group and displaying the characteristic (501) reflection at $2\theta \sim 23^{\circ}$. [48] The second most abundant phase is amorphous silica (35.6 wt.%), recognizable by the broad diffuse reflection in the $15 < 2\theta < 30^{\circ}$ range. The third and the final silicon oxide phase detected, with 21.8 wt.%, is that of combeite ($Na_2Ca_2Si_3O_9$), which crystallizes in the trigonal structure and $P3_121$ space group. And because the amount of the crystalline phases outweighed the amorphous content, the material represents a glass-ceramic rather than a classical glass. As per the Debye–Scherrer equation (Eq. (1)), the average crystallite size – i.e., the coherence length, to be more precise - for the amorphous component equaled 2.47 nm, while the corresponding size of the crystalline domains for the two crystalline components, silicalite-1 and combeite, was in the 20–40 nm range. The addition of chitosan led to the appearance of the two characteristic reflections [49]: (020) at $2\theta \sim 10^{\circ}$ and (110) at $2\theta \sim 20^{\circ}$. Both reflections were relatively weak and broad, signifying low crystallinity and not an excessively high weight content in the nanocomposite.

Table 2 Contribution of individual doped silicon oxide phases to the total composition of the bioglass-ceramic component of the nanocomposite, as calculated by comparing their respective integrated diffraction peak intensities

Component	Space group	Percent of composition (wt.%)
Amorphous glass	/	35.6
Silicalite-1	Pnma	42.6
Combeite	$P3_121$	21.8

The FTIR analysis was conducted on pure bioglass-ceramic samples undoped or doped with Nb and/or Zn, and on Nb-doped bioglass-ceramic hybridized with chitosan. The bioglass-ceramic was characterized by three prominent bands, which originated from the stretching Si–O and bending Si–O–Si vibration modes, the former of which manifested as bands at 1053 and 800 cm^{-1} and the latter of which manifested as the band at 447 cm^{-1} (Fig. 6a). The analysis demonstrated no extreme effects of the dopant presence, identity or concentration on the spectra as compared to the original bioglass-ceramic (Fig. 6a). Correspondingly, both Nb- and Zn-doped bioglass-ceramics produced what appeared at first sight as indistinct spectra when compared to the spectrum of the control, undoped bioglass-ceramic (Fig. 6a). However, a more detailed analysis of the wavenumber shift and full-width at half maxima (FWHM) of the infrared bands showed that there were evident effects of the presence, concentration and chemical identity of the ionic dopant. Thus, for example, while no significant peak shifts were noticed in the spectrum of the bioglass-ceramic doped with a lower, 0.05 M concentration of Zn compared to the control bioglass-ceramic, a consistent upshift to higher wavenumbers was noticed for the higher, 0.1 M concentration of Zn. Specifically, this upshift amounted to 10.1 cm^{-1} for the Si–O stretching mode centered at 1053 cm^{-1} in the undoped control (Fig. 6b) and 1.5 cm^{-1} for the Si–O–Si bending mode centered at 447 cm^{-1}. The addition of Nb produced a similar, but milder effect on the upshift of the Si–O stretching mode, increasing its frequency by 6.1 cm^{-1} at the 0.1 M concentration of Nb as compared to the undoped control (Fig. 6b).

An increase of the frequency of the stretching modes normally indicates a greater degree of independence of the active group and a lesser overlap of its electron density with the surrounding modes. One effect by which this can be achieved is through modifying the crystallinity and the concentration of voids (i.e., broken bonds in the network) in the amorphous structure. The amorphous structure is usually less densely packed than its crystalline analog and it is conceivable that Nb and Zn hampered the partial recrystallization taking place during annealing by interfering with the Si–O network restructuring, thus leaving the structure more open than in their absence. This mechanism

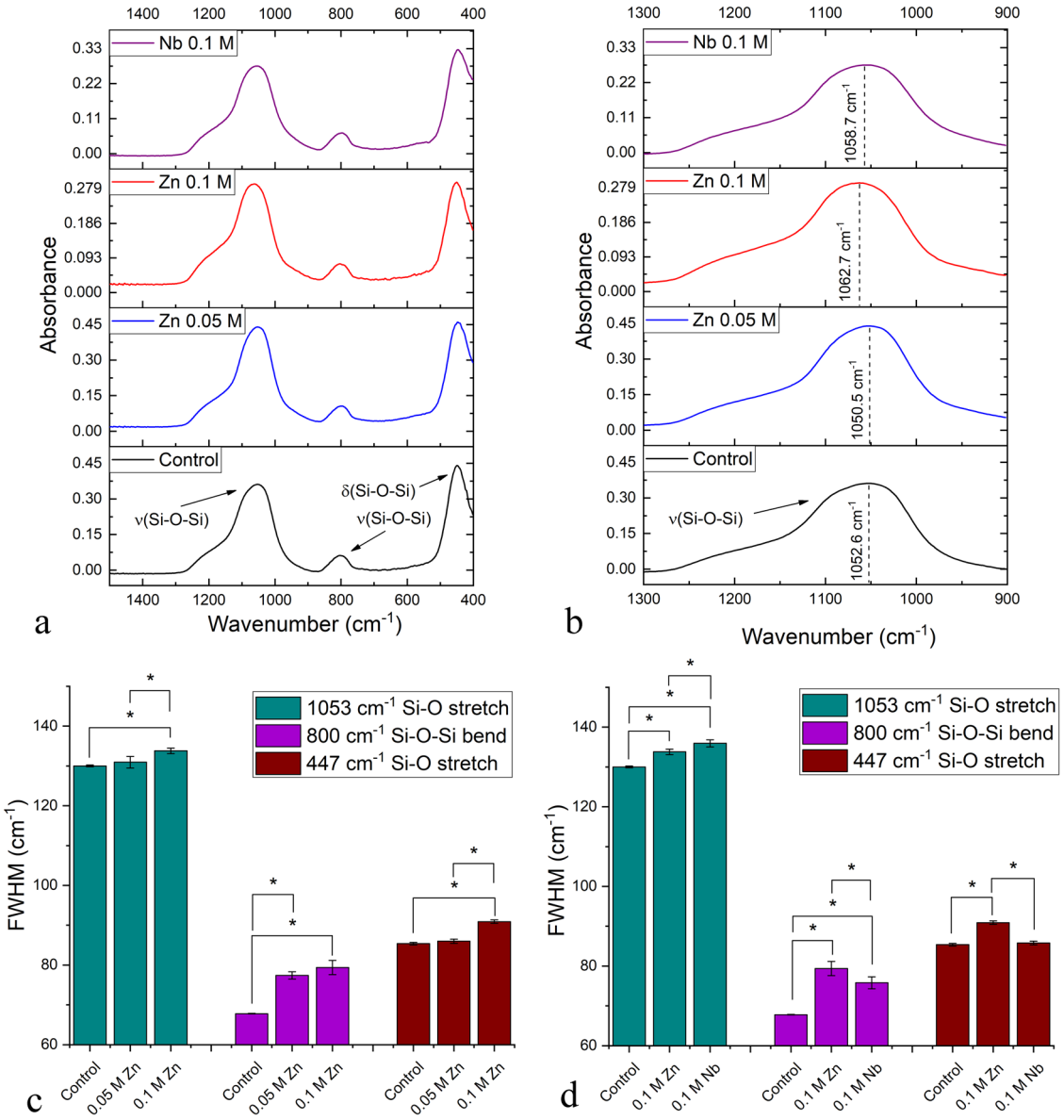

Fig. 6 FTIR spectra of different bioglass-ceramic samples, including the control, undoped sample and samples doped with different concentrations of niobium and zinc ions, focusing on the entire 1500–400 cm^{-1} spectral region recorded (**a**), and on the Si–O–Si stretching mode at ~1053 cm^{-1} (**b**). FWHM values for the three main vibration modes in the FTIR spectrum of the bioglass-ceramic as a function of the concentration of Zn ions in it (**c**), and as a function of the chemical identity of the ionic dopant (Zn or Nb) (**d**)

is confirmed by the trend in the FWHM change for all the three major Si–O(–Si) vibrational modes upon the addition of the ionic dopants, i.e., Nb and/or Zn. FWHM of the absorption bands is inversely proportional to crystallinity, so that broadening of these bands effectively corresponds to reduced crystallinity [50], a consequence of the broader distribution of stereochemical environments surrounding the active vibrational modes [51, 52].

Overall, with the addition of Zn at the higher concentration of 0.1 M, the FWHM increased by 1.5–6% depending on the vibration mode. However, for all the three major Si–O(–Si) vibration modes, the FWHM increased in direct proportion with the amount of Zn ions accommodated inside the lattice of the bioglass-ceramic (Fig. 6c). A comparison between the FWHM values of the three major vibration modes in the spectra of the bioglass-ceramic samples doped with Zn or Nb showed that both dopants increased the FWHM as the consequence of their acting as structure-breakers and reducing the crystallinity of the annealed bioglass-ceramic, with the effect of Zn being slightly more intensive than that of Nb (Fig. 6d). This difference may be traced to the fact that Nb is pentavalent and may substitute silicon ions in the glassy backbone with a lesser degree of structural disruption than that resulting

from the incorporation of divalent Zn ions. No bands other than the Si–O(–Si) ones appeared in the spectra of any of the doped bioglass-ceramic samples, indicating no formation of secondary phases, such as ZnO or any of niobium oxides (Fig. 6a), which is consistent with the results of the diffractometric analysis.

Successful hybridization of the bioglass-ceramic with chitosan was also demonstrated with the use of FTIR. Whereas the use of 1:50 weight ratio of chitosan vs. bioglass-ceramic did not show any prominent bands originating from the organic phase (data not shown for brevity reasons), the use of ten times higher, 1:5 weight ratio between the two components resulted in a number of prominent chitosan bands, as shown in Fig. 7a–d. In particular, Fig. 7a shows the presence of the C–O stretch centered at 1030 cm^{-1} and partially overlapping with the antisymmetric Si–O–Si stretch of the bridging oxygen at 1052 cm^{-1}. The C–O–C stretch was detected at 1148 cm^{-1} and the C–O bending, deformation mode at 1376 cm^{-1}, confirming the presence of chitosan. The addition of chitosan also increased the hygroscopic character of the material, as confirmed by the appearance of a strong O–H stretch peaking at 3320 cm^{-1} and originating from the adsorbed water molecules (Fig. 7b). In contrast, no such band was present in the control bioglass-ceramic, be it doped or undoped (Fig. 7b). The weak shoulder in the lower frequency range of this band originated from the C–H stretch, yet another band derived from the chitosan component (Fig. 7b). The strong bending amine vibration was detected at 1638 cm^{-1}, being typical for the aminated chitosan molecules, expectedly absent in the control sample (Fig. 7c). The broad H–C=O carbonyl bending mode, originating from the acetyl groups, was detected in the 550–650 cm^{-1} region (Fig. 7d).

TEM imaging demonstrated an intimate interaction between the bioglass-ceramic and the polymeric component of the material, while a direct confirmation of it in the FTIR analysis came from the observed downshift of the critical Si–O–Si vibrations upon the addition of chitosan. This shift is illustrated in Fig. 7d, equaling 31 cm^{-1} for the Si–O–Si bend at 447 cm^{-1} and 17 cm^{-1} for the symmetric stretch of the three siloxane rings of SiO_4 centered at 800 cm^{-1}. Typically, as an atomic group is brought to interaction with another chemical group, its actively vibrating bond becomes lengthened, leading to a corresponding downshift in the infrared band.

Finally, to test the potential of the material for biological application, the analysis of the viability of MDPC-23 odontoblast-like cells and antimicrobial activity in response to doped and undoped bioglass-ceramics was conducted and the results are presented in Fig. 8 and Fig. 9, respectively. The viability assays were conducted in a rather broad particle concentration range of 0.1–10,000 µg/mL and the cell viability was unaffected by any particles, be they undoped or doped, until the concentration limit of 10 µg/mL was exceeded. At 100 µg/mL, the only sample for which the viability was statistically significantly lowered compared to the control cells treated with no particles was the Zn-doped bioglass-ceramic (Fig. 8a). This trend according to which the cells were most adversely affected by the Zn-doped bioglass-ceramic was reflected in the corresponding IC_{50} values, which were identical for the control, undoped bioglass-ceramic and for the Nb-doped glass-ceramic: 2.5 mg/mL (Fig. 8b, d). However, at 1.9 mg/mL, the IC_{50} value was lower for the Zn-doped glass-ceramic (Fig. 8c), indicating the susceptibility of the odontoblast-like cells to the presence of Zn ions in the material at its lower doses. It is conceivable that the cells would react equally or even more intensely to Nb ions had their concentration in the Nb-doped glass-ceramic not been an order of magnitude lower than that of Zn ions in the Zn-doped glass-ceramic (Table 1). At higher doses, however, an interesting effect occurred, where the viability of cells challenged with the Zn-doped glass-ceramic - to which the cells were more susceptible at lower doses – became higher than that of the cells treated with the control, undoped bioglass-ceramic or with the Nb-doped glass-ceramic (Fig. 8a). Eventually, at the highest dose of 10 mg/mL, the viability of cells treated with the undoped, control material became lower than the viability of cells treated with either Zn- or Nb-doped bioglass-ceramic (Fig. 8a), hinting at the completely viable effect of the two dopants at the higher doses. In the antimicrobial in vitro assay, the test compound did not significantly affect *S. mutans* viability (Fig. 9) and the MIC and MBC results were not significantly different among groups ($p > 0.05$, data not shown).

Prior studies have shown that the effect of Zn added to bioactive glass nanoparticles is cell-dependent, increasing the viability of cells such as MG-63 osteosarcoma cells, but decreasing the viability of cells such as embryonic fibroblasts in the 0.1–5 mg/ml concentration range [53]. Increasing the concentration of Zn in bioactive glasses past a certain limit also led to a proportional decrease in the viability of dendritic cells [54]. In contrast, the addition of Nb ions to 45S5 bioglass of the same basic composition as that used in this study up to 1.3 at.% did not produce any adverse effects on human embryonic stem cells for incubations reaching up to 14 days in duration [55]. All of this makes the biological aspect of the results of this study in agreement with the literature findings. Simultaneously, the addition of either Zn or Nb to bioactive glass had a positive effect on the osteogenic behavior of osteoblast-like cells, if not on the cell proliferation [56, 57]. A whole separate question is why the cells appear to be more affected by Zn than by Nb ions if Zn is an essential microelement and one of the most common dopants in materials for bone and

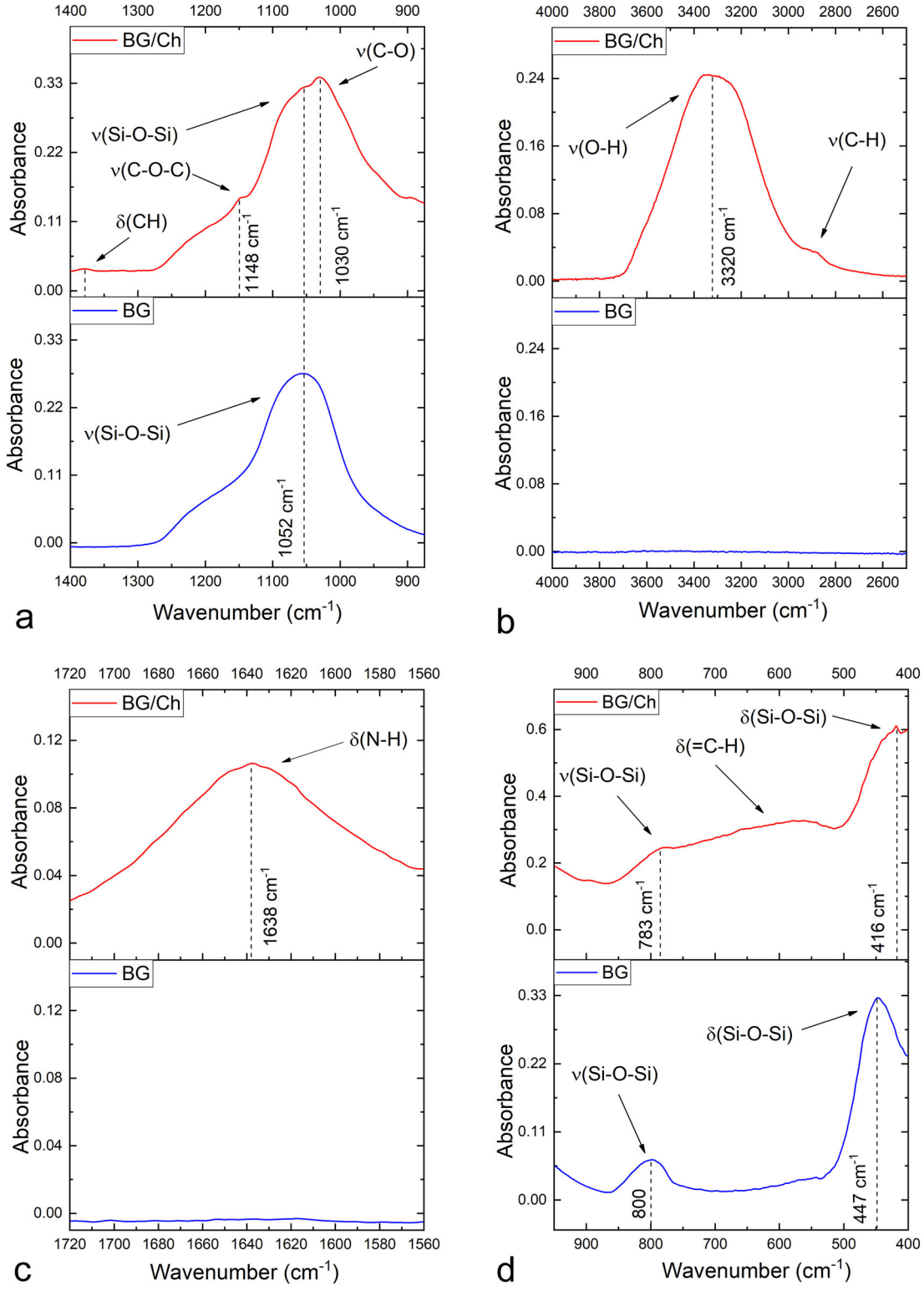

Fig. 7 FTIR spectra of control, undoped bioglass-ceramic (BG) and of chitosan-coated (BG/Ch) niobium-doped bioglass-ceramic in different spectral regions, including the denotations of the most prominent vibration modes: 1400–875 cm^{-1} (**a**), 4000–2500 cm^{-1} (**b**), 1720–1560 cm^{-1} (**c**), and 950–400 cm^{-1} (**d**)

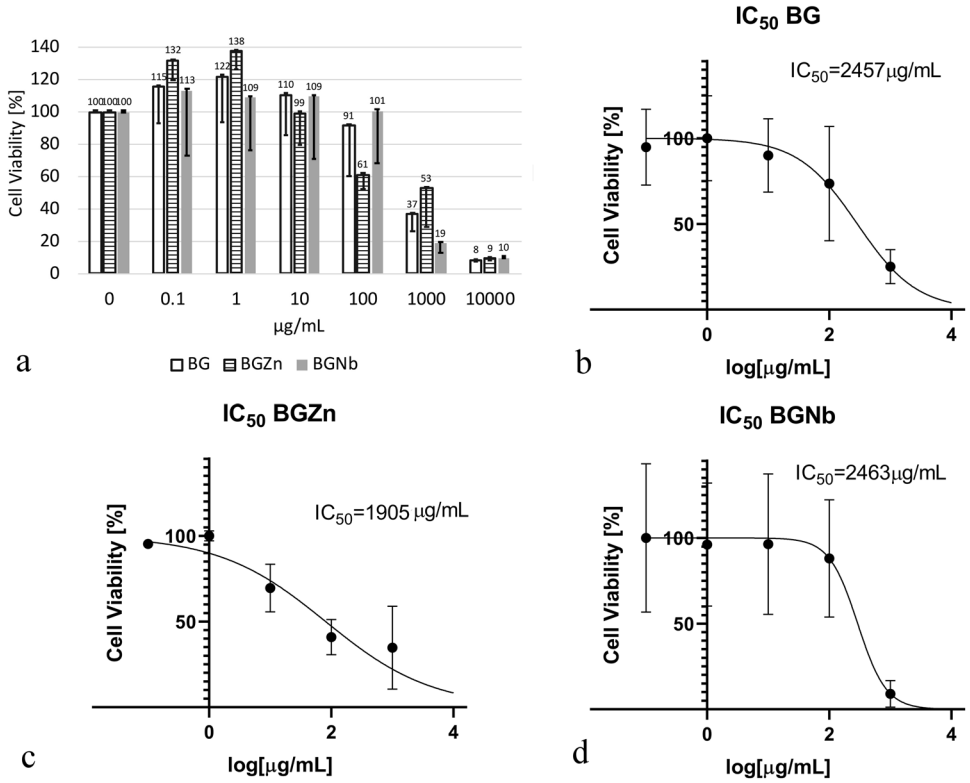

Fig. 8 Viabilities of MDPC-23 odontoblast-like cells challenged for 24 h with different doses of control, undoped bioglass-ceramic nanoparticles (BG) and of bioglass-ceramic nanoparticles doped with Zn (BGZn) of Nb (BGNb) and normalized to the viability of the negative control cells challenged with no particles (**a**), along with the IC50 values for BG (**b**), BGZn (**c**) and BGNb (**d**) calculated from the viability vs. dose curves plotted on the logarithmic scale. Bars and dots are data points derived from multiple experimental and measurement replicas, while error bars represent standard deviation

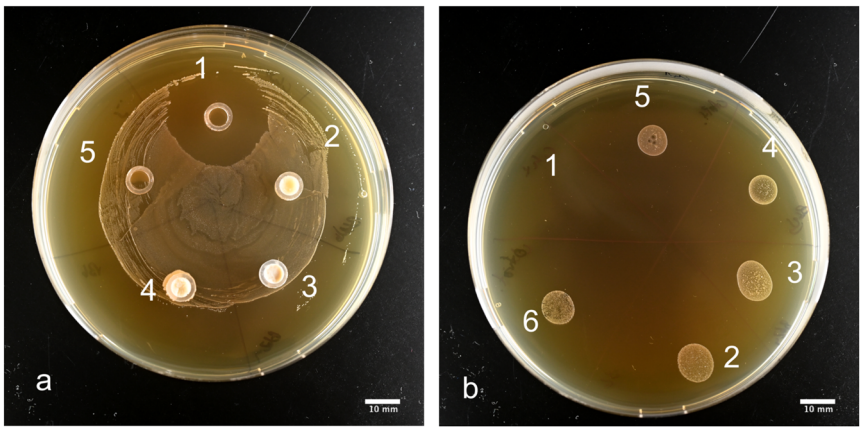

Fig. 9 **a** Representative digital image ($n = 12$) of a Petri dish with Trypsin Soy Agar for 48 h and 10^5 CFU/mL of *Streptococcus mutans* depicting the inhibition halo for all experimental groups: (1) chlorhexidine 0.12% 10 μL; (2) control, undoped bioglass-ceramic 10 mg; (3) Zn-doped bioglass-ceramic 10 mg; (4) Nb-doped bioglass-ceramic 10 mg; (5) chitosan-hybridized control, undoped bioglass-ceramic 10 mg. **b** Representative digital image ($n = 12$) of a Petri dish with Trypsin Soy Agar and aliquots of 10 μL of Trypsin Soy Agar broths inoculated with 10^5 CFU/mL of *Streptococcus mutans* after 24 h of incubation with different experimental groups: (1) chlorhexidine 0.12% 10 μL; (2) control, undoped bioglass-ceramic 10 mg; (3) Zn-doped bioglass-ceramic 10 mg; (4) Nb-doped bioglass-ceramic 10 mg; (5) chitosan-hybridized control, undoped bioglass-ceramic 5 mg; (6) 10^5 CFU/mL of *Streptococcus mutans*

dental tissue replacement [4], whereas Nb is foreign to the human body and has no known functions in it. Despite that, Nb falls in the category of metals that are no more toxic to humans than the metals traditionally used in orthopedic and dental biomaterials [58], such as Al, Cr, Fe, Mo, and Zr, which encourages its continued research for applications in dental science.

As far as the antibacterial activity is concerned, the bioglass-ceramic, with or without Zn and Nb dopants, did not display any measurable bactericidal activity against *S. mutans* in the agar plate assay (Fig. 9). The only measurable activity was obtained for the positive control, chlorhexidine, equivalent to the inhibition zone of 9.2 ± 0.3 mm. The MIC and the MBC for all types of the

bioglass-ceramic exceeded 10 mg/ml, suggesting that the bioglass-ceramic may not be able to suppress the infectious caries disease through ion-doping, let alone without it. Hybridization with chitosan did not provide for any measurable increase in the antibacterial activity against *S. mutans* either (Fig. 9). It is likely that the high-temperature treatment reduced the solubility of the nanoparticles and release rate of the antibacterial ions, for which reason the optimization of this treatment may be needed to endow the particles with the antibacterial activity. As for the effect of chitosan, it is possible that different assays - including the biofilm vitality, the plaque regrowth, and other - would yield more positive results, which would be in agreement with earlier reports on the ability of this polymer to inhibit *S. mutans* [59, 60]. Also, it is possible that despite the lack of activity against *S. mutans*, the particles may exhibit activity against other bacteria implicated in the infection of oral cavity. All in all, futher studies are needed to optimize the nanoparticles for a more potent cariostatic activity and investigate their influence on the virulence factors *S. mutans* and other relevant bacterial species, along with the potential for remineralization of enamel and dentin.

4 Conclusions

The goal of this study was to synthesize and characterize Zn–Nb bioglass-ceramic/chitosan nanoparticles for future incorporation in remineralizing solutions, preventive and restorative dental materials, regenerative endodontic sealers, and bone scaffolds. This particular goal is a subset of a broader goal, which is to develop the new and/or improve on the existing biomimetic approaches for minimally invasive dentistry. One such approach we are pursuing relies on the effective deep penetration of nanoparticles into affected tissues accompanied by the slow release of antimicrobial and remineralizing ions, thus healing the disease-affected tissues.

To that end, we successfully synthesized monodisperse Na_2O–CaO–P_2O_5–SiO_2 chitosan-hybridized bioglass-ceramic nanoparticles doped with antibacterial, mineralizing and osteogenic Zn and Nb ions. Such compositionally complex composites were characterized for their particle size, morphology, phase composition and bioglass-ceramic/polymer interface with a range of physicochemical characterization techniques. The results of TEM and FTIR analyses demonstrated a continuous and intimate interface between bioglass-ceramic nanoparticles and chitosan on the atomic and the nano scales. Both Zn and Nb ions hindered the recrystallization process of the glassy phase, but had no significant effect on hybridization with chitosan. The effective electrostatic attraction between the aminated hydrocarbon chains of chitosan and the negatively charged silanol groups of silica may extend to the interaction between the biomaterial and dentin collagen fibrils decalcified due to caries, making the material of potential interest for incorporation into adhesive systems, solutions and restorative materials. In spite of exhibiting no antibacterial activity against caries-causing *S. mutans*, the material was shown to interact favorably with odontoblast-like cells, accentuating its potential for further research for applications in minimally invasive reparative dentistry.

Acknowledgements This work was performed in part at the Analytical Instrumentation Facility (AIF) at North Carolina State University, which is supported by the State of North Carolina and the National Science Foundation (award number ECCS-2025064). The AIF is a member of the North Carolina Research Triangle Nanotechnology Network (RTNN), a site in the National Nanotechnology Coordinated Infrastructure (NNCI). Part of this research was supported by an East Carolina University faculty startup award to SG.

Author contributions VU, LG and SG conceptualized the study. PRBdC, FCPP-d-S and MACS synthesized the bioglass ceramic. VU and VMW synthesized the bioglass ceramic/chitosan hybrid. VU performed the diffractometric and spectroscopic characterizations and analyses. SG performed the TEM analysis. GA performed the biological characterization under the supervision of VU, VMW, RMM and SG. VU interpreted the data and wrote the paper with the input from LG and SG. SG supervised the project.

Compliance with ethical standards

Conflict of interest The authors declare that they have no conflict of interest.

Publisher's note Springer Nature remains neutral with regard to jurisdictional claims in published maps and institutional affiliations.

References

1. Hemeg HA (2017) Nanomaterials for alternative antibacterial therapy. Int J Nanomed 12:8211–8225
2. Uskoković V, Tang S, Nikolić MG, Marković S, Wu VM (2019) Calcium phosphate nanoparticles as intrinsic inorganic antimicrobials: in search of the key particle property. Biointerphases 14:031001
3. Rau JV, Wu VM, Graziani V, Fadeeva IV, Fomin AS, Fosca M, Uskoković V (2017) The bone building blues: self-hardening copper-doped calcium phosphate cement and its in vitro assessment against mammalian cells and bacteria. Mater Sci Eng C 79:270–279
4. Uskoković V (2020) Ion-doped hydroxyapatite: an impasse or the road to follow? Ceram Int 46:11443–11465
5. Ferracane JL (2013) Resin-based composite performance: are there some things we can't predict? Dent Mater 29:51–58
6. Uskoković V, Bertassoni LE (2010) Nanotechnology in dental sciences: moving towards a finer way of doing dentistry. Materials 3:1674–1691
7. Uskoković V (2015) When 1+1>2: nanostructured composite materials for hard tissue engineering applications. Mater Sci Eng C 57:434–451
8. Wilson J, Clark AE, Hall M, Hench LL (1993) Tissue response to Bioglass endosseous ridge maintenance implants. J Oral Implantol 19:295–302

9. de Morais RC, Silveira RE, Chinelatti M, Geraldeli S, de Carvalho Panzeri Pires-de-Souza F (2018) Bond strength of adhesive systems to sound and demineralized dentin treated with bioactive glass-ceramic suspension. Clin Oral Investig 22:1923–1931
10. Kokubo T, Takadama H (2006) How useful is SBF in predicting in vivo bone bioactivity? Biomaterials 27:2907–2915
11. Kaur G, Pandey OP, Singh K, Homa D, Scott B, Pickrell G (2014) A review of bioactive glasses: their structure, properties, fabrication and apatite formation. J Biomed Mater Res A 102:254–274
12. Baino F, Hamzehlou S, Kargozar S (2018) Bioactive glasses: where are we and where are we going? J Funct Biomater 9:25
13. Ignjatović NL, Sakač M, Kuzminac I, Kojić V, Marković S, Vasiljević-Radović D, Wu VM, Uskoković V, Uskoković DP (2018) Chitosan oligosaccharide lactate coated hydroxyapatite nanoparticles as a vehicle for the delivery of steroid drugs and the targeting of breast cancer cells. J Mater Chem B 6:6957–6968
14. Ali A, Ahmed S (2018) A review on chitosan and its nanocomposites in drug delivery. Int J Biol Macromolecules 109:273–286
15. Saita K, Nagaoka S, Shirosaki T, Horikawa M, Ihara H (2020) Dispersible chitosan particles showing bacteriostatic effect against Streptococcus mutans and their dental polishing effect. Biosci Biotechnol Biochem 84:1265–1273
16. Rajabnia R, Ghasempour M, Gharekhani S, Gholamhoseinnia S, Soroorhomayoon S (2016) Anti -Streptococcus mutans property of a chitosan: containing resin sealant. J Int Soc Prev Community Dent 6:49–53
17. Chen C-Y, Chung Y-C (2012) Antibacterial effect of water-soluble chitosan on representative dental pathogens Streptococcus mutans and Lactobacilli brevis. J Appl Oral Sci 20:620–627
18. Trindade CEP (2007) Microelements and vitamins in the nutrition of very low-birthweight preterm infants: a Brazilian perspective. NeoReviews 8:3–13
19. Wada O (2004) What are trace elements?—Their deficiency and excess states. JMAJ 47:351–358
20. Pasquet J, Chevalier Y, Pelletier J, Couval E, Bouvier D, Bolzinger M-A(2014) The contribution of zinc ions to the antimicrobial activity of zinc oxide Colloids Surf A 457:263–274
21. Mohammed NR, Mneimne M, Hill RG, Al-Jawad M, Lynch RJ, Anderson P (2014) Physical chemical effects of zinc on in vitro enamel demineralization. J Dent 42:1096–1104
22. Mayer I, Apfelbaum F, Featherstone JD (1994) Zinc ions in synthetic carbonated hy-droxyapatites. Arch Oral Biol 39:87–90
23. Mohammed NR, Lynch RJ, Anderson P (2015) Inhibitory effects of zinc ions on enamel demineralisation kinetics in vitro. Caries Res 49:600–605
24. Dybowska A, Manning DA, Collins MJ, Wess T, Woodgate S, Valsami-Jones E (2009) An evaluation of the reactivity of synthetic and natural apatites in the presence of aqueous metals. Sci Total Environ 407:2953–2965
25. Williams RAD, Elliott JC (1989) Chemistry of the calcium phosphates. In: Basic and applied dental biochemistry, Churchill Livingstone, Edinburgh/London/New York, pp 318–341
26. Lynch RJ, Butler A, Kearns S (2015) Effect of zinc and fluoride on secondary demineralisation of enamel lesions in vitro. Caries Res 49:357
27. Lynch RJM, Duckworth RM (2020) Microelements: Part I: Zn, Sn, Cu, Fe and I. In: Zohoori FV, Duckworth RM (eds) The impact of nutrition and diet on oral health. Monographs in Oral Science. Karger, Basel, vol. 28, pp 32–47
28. Hoppe A, Mouriño V, Boccaccini AR (2013) Therapeutic inorganic ions in bioactive glasses to enhance bone formation and beyond. Biomater Sci 1:254–256
29. Balamurugan A, Balossier G, Kannan S, Michel J, Rebelo AH, Ferreira JM (2007) Development and in vitro characterization of sol–gel derived CaO–P2O5–SiO2–ZnO bioglass. Acta Biomaterialia 3:255–262
30. Wahono NA, Ford D, Wakeling LA, Valentine RA (2019) The presence and response to Zn of ZnT family mRNAs in human dental pulp. Metallomics 11:613–620
31. Berès F, Isaac J, Mouton L, Rouzière S, Berdal A, Simon S, Dessombz A (2016) Comparative physicochemical analysis of pulp stone and dentin. J Endod 42:432–438
32. Yao T, Chen J, Wang Z, Zhai J, Li Y, Xing J, Hu S, Tan G, Qi S, Chang Y, Yu P, Ning C (2019) The antibacterial effect of potassium-sodium niobate ceramics based on controlling piezoelectric properties. Colloids Surf B Biointerfaces 175:463–468
33. de Souza E, Silva JM, Pastorello M, Kobarg J, Cardoso MB, Mazali IO (2013) Selective synthesis of silver nanoparticles onto potassium hexaniobate: structural organisation with bactericidal properties. ChemPhysChem 14:4075–4083
34. Beherei HH, Shaltout AA, Mabrouk M, Abdelwahed NAM, Das DB (2018) Influence of niobium pentoxide particulates on the properties of brushite/gelatin/alginate membranes. J Pharm Sci 107:1361–1371
35. Palasuk J, Windsor LJ, Platt JA, Lvov Y, Geraldeli S, Bottino MC (2018) Doxycycline-loaded nanotube-modified adhesives inhibit MMP in a dose-dependent fashion. Clin Oral Investig 22:1243–1252
36. Clinical and Laboratory Standards Institute (2015). Methods for antimicrobial dilution and disk susceptibility testing of infrequently isolated or fastidious bacteriai. 3rd ed. CLSI guideline M45. PA: Clinical and Laboratory Standards Institute, Wayne
37. Wan Q, Sheffield J, McCool J, Baran G (2008) Light curable dental composites designed with colloidal crystal reinforcement. Dent Mater 24:1694–701
38. Lin Z, Wu J, Qiao W, Zhao Y, Wong KHM, Chu PK, Bian L, Wu S, Zheng Y, Cheung KMC, Leung F, Yeung KWK (2018) Precisely controlled delivery of magnesium ions through sponge-like monodisperse PLGA/nano-MgO-alginate core-shell microsphere device to enable in-situ bone regeneration. Biomaterials 174:1–16
39. Uskoković V (2020) Factors defining the stability of poly(lactide-co-glycolide) spheres for the sustained release of a cysteine protease inhibitor. Int J Pharmaceutics 583:119316
40. de Lima CLJ, Pastena B, RPRD Nardi, JTG Junior, Ferrari JL, Cassanjes FC, Poirier F (2015) Thermal, structural and crystallization study of niobium potassium phosphate glasses. Mat Res 18:13–16
41. Ahmad M, Aly K, Saddeek YB, Dahshan A (2020) Glass transition and crystallization kinetics of Na_2O–B_2O_3–Nb_2O_5–Bi_2O_3 ceramic glasses. J Non-Crystalline Solids 546:120260
42. Zhao M, Gao J, Shi Y, Li B-W (2020) Effect of niobium pentoxide (Nb_2O_5) on the microstructure and properties of the diopside glass-ceramics produced from Bayan Obo mine tailing. J Aust Ceram Soc 56:1079–1087
43. Stunda A, Jakovlevs D, Poca L, Berzina-Cimdina L (2012) Surface morphology of P2O5-CaO-Nb2O5-Na2O glass-ceramics after acid treatment: SEM and XRD study. Key Eng Mater 493/4:61–67
44. Du X, Liu Y, Yan H, Rafique M, Li S, Shan X, Wu L, Qiao M, Kong D, Wang L (2020) Anti-infective and pro-coagulant chitosan-based hydrogel tissue adhesive for sutureless wound closure. Biomacromolecules 21:1243–1253
45. Mati-Baouche N, Delattre C, de Baynast H, Grédiac M, Mathias JD, Ursu AV, Desbrières J, Michaud P (2019) Alkyl-chitosan-based adhesive: water resistance improvement. Molecules 24:10
46. Shi C, Chen X, Zhang Z, Chen Q, Shi D, Kaneko D (2020) Mussel inspired bio-adhesive with multi-interactions for tissue repair. J Biomater Sci Polym Ed 31:491–503
47. Geraldeli S, Soares EF, Alvarez AJ, Farivar T, Shields RC, Sinhoreti MAC, Nascimento MM (2017) A new arginine-based

dental adhesive system: formulation, mechanical and anti-caries properties. Dent 63:72–80
48. Alfaro S, Valenzuela M, Bosch P (2008) Synthesis of silicalite-1 by dry-gel conversion method: factors affecting its crystal size and morphology. J Porous Mater 16:337–342
49. Hai TAP, Sugimoto R (2018) Fluorescence control of chitin and chitosan fabricated via surface functionalization using direct oxidative polymerization. RSC Adv 8:7005–7013
50. Amenta E, King HE, Petermann H, Uskoković V, Tommasini SM, Macica CM (2018) Vibrational spectroscopic analysis of hydroxyapatite in HYP mice and individuals with XLH. Therapeutic Adv Chronic Dis 9:268–281
51. Uskoković V (2019) Disordering the disorder as the route to a higher order: incoherent crystallization of calcium phosphate through amorphous precursors. Cryst Growth Des 19:4340–4357
52. Uskoković V (2020) Visualizing different crystalline states during the infrared imaging of calcium phosphates. Vibrational Spectrosc 107:103045
53. Neščakova Z, Zheng K, Liverani L, Nawaz Q, Galuskova D, Kankova H, Michalek M, Galusek D, Boccaccini AR (2019) Multifunctional zinc ion doped sol-gel derived mesoporous bioactive glass nanoparticles for biomedical applications. Bioact Mater 4:312–321
54. Schuhladen K, Stich L, Schmidt J, Steinkasserer A, Boccaccini AR, Zinser E (2020) Cu, Zn doped borate bioactive glasses: antibacterial efficacy and dose-dependent in vitro modulation of murine dendritic cells. Biomaterial. Science 8:2143–2155
55. Souza L, Lopes JH, Encarnacao D, Mazali IO, Martin RA, Camilli JA, Bertran CA (2018) Comprehensive in vitro and in vivo studies of novel melt-derived Nb-substituted 45S5 bioglass reveal its enhanced bioactive properties for bone healing. Sci Rep. 8:12808
56. Du RL, Chang J, Ni SY, Zhai WY, Wang JY (2006) Characterization and in vitro bioactivity of zinc-containing bioactive glasses and glass-ceramics. J Biomater Appl 20:341–360
57. Obata A, Takahashi Y, Miyajima T, Ueda K, Narushima T, Kasuga T (2012) Effects of niobium ions released from calcium phosphate invert glasses containing Nb2O5 on osteoblast-like cell functions. ACS Appl Mater Interfaces 4:5684–5690
58. Hallab N, Anderson S, Caicedo M, Jacobs J (2006) Zirconium and niobium affect human osteoblasts, fibroblasts, and lymphocytes in a similar manner to more traditional implant alloy metals. In: Zardiackas L, Freese H, and Kraay M (eds) Titanium, niobium, zirconium, and tantalum for medical and surgical applications. ASTM International, West Conshohocken, PA, pp 248–259
59. Pasquantonio G, Greco C, Prenna M, Ripa C, Vitali LA, Petrelli D, Di Luca MC, Ripa S (2008) Antibacterial activity and antibiofilm effect of chitosan against strains of Streptococcus mutans isolated in dental plaque. Int J Immunopathol Pharm 21:993–997
60. Bae K, Jun EJ, Lee SM, Paik DI, Kim JB (2006) Effect of water-soluble reduced chitosan on Streptococcus mutans, plaque regrowth and biofilm vitality. Clin Oral Invest 10:102–107